



Effects of paramagnetic $[\text{Fe}(\text{C}_5\text{Me}_5)_2]^+$ cation on the anionic single-molecule magnet, $[\text{Mn}_{12}\text{O}_{12}(\text{O}_2\text{CC}_6\text{H}_4\text{F}(-o))_{16}(\text{H}_2\text{O})_4]^-$

Takayoshi Kuroda-Sowa ^{a,1}, Motohiro Nakano ^{a,2}, George Christou ^b,
David N. Hendrickson ^{a,*}

^a Department of Chemistry and Biochemistry-0358, University of California at San Diego, La Jolla, CA 92093-0358, USA

^b Department of Chemistry, Indiana University, Bloomington, IN 47405, USA

Received 17 September 2000; accepted 15 October 2000

Abstract

The preparation and physical characterization are reported for the single-molecule magnet salts $A[\text{Mn}_{12}\text{O}_{12}(\text{O}_2\text{CC}_6\text{H}_4\text{F}(-o))_{16}(\text{H}_2\text{O})_4]$ ($A^+ = \text{PPh}_4^+$ (**2a**), $\text{Fe}(\text{C}_5\text{Me}_5)_2^+$ (**2b**), and $\text{Co}(\text{C}_5\text{Me}_5)_2^+$ (**2c**)). The effects of the magnetic cation on the magnetization relaxation behavior of the $[\text{Mn}_{12}]^-$ anions are investigated. All complexes exhibit out-of-phase ac magnetic susceptibility (χ''_M) signals in the 4.8–5.1 K range at 1 kHz ac frequency. The temperature of the χ''_M peaks is frequency dependent, as expected for a single-molecule magnet. From Arrhenius plots of the frequency dependence of the temperature of the χ''_M peaks, the effective energy barriers U_{eff} for changing the magnetization direction from spin “up” to spin “down” were estimated to be in the 52–57 K range. Magnetization hysteresis loops were observed for all the complexes studied. They show clear hysteresis loops with steps, indicating the effect of the magnetic cation on the magnetization relaxation of the anionic $[\text{Mn}_{12}]^-$ complex is rather small. The least-squares fittings of variable-field magnetization data show the ground state of complex **2a** is best described as $S = 21/2$ with $g = 1.96$ and $D = -0.56$ K, while complexes **2b** and **2c** have $S = 19/2$ ground states. The fitting parameters are $g = 1.96$ and $D = -0.54$ K for complex **2b** and $g = 1.95$ and $D = -0.57$ K for complex **2c**. These analyses show the magnetic cation has essentially no effect on the ground state spin or on the parameters g and D for the $[\text{Mn}_{12}]^-$ anion. © 2001 Elsevier Science Ltd. All rights reserved.

Keywords: Single-molecule magnet; $[\text{Mn}_{12}]^-$ complex anion; Hysteresis; Quantum tunneling of magnetization; ac and dc magnetic susceptibility; Metallocene cation

1. Introduction

There is considerable growing interest in single-molecule magnets (SMMs) [1,2]. The first molecule shown to be a SMM is the 12-nuclei manganese complex $[\text{Mn}_{12}\text{O}_{12}(\text{OAc})_{16}(\text{H}_2\text{O})_4]$ (**1**) [3–8]. Due to its large-spin ground state ($S = 10$) together with the uniaxial magnetic anisotropy (due to zero-field splitting D), each molecule has a potential barrier of $|D|S^2$ for reversal of the direction of its magnetization. This

barrier leads to a magnetization hysteresis loop and the appearance of an out-of-phase signal in the ac susceptibility at low temperatures, where $k_B T$ is considerably smaller than the barrier height.

Although it has been shown that these interesting properties arise from isolated molecules, it is also important to investigate how the environment around the $[\text{Mn}_{12}]$ SMMs affects them. Recently, the magnetic properties of $[m\text{-MPYNN}][\text{Mn}_{12}\text{O}_{12}(\text{O}_2\text{CPh})_{16}(\text{H}_2\text{O})_4]$ have been reported by Takeda and Awaga [9] where $[m\text{-MPYNN}]^+$ is the organic cation radical *m*-*N*-methylpyridinium nitronylnitroxide. On the basis of the X-band EPR measurements and the observation of ac magnetization relaxation, they concluded that the organic radical with $S = 1/2$ enhances the magnetization relaxation of the $[\text{Mn}_{12}]^-$ complex and reduces the blocking temperature of the anion.

* Corresponding author.

¹ Present address: Department of Chemistry, Kinki University, 3-4-1, Kowakae, Higashi-Osaka, 577-8502, Japan.

² Present address: Applied Chemistry Division, Graduate School of Engineering, Osaka University, 1-16, Machikaneyama, Toyonaka, Osaka 560-0043, Japan.

In order to investigate this point more thoroughly, the complex $[\text{Mn}_{12}\text{O}_{12}(\text{O}_2\text{CC}_6\text{H}_4\text{F}(-o))_{16}(\text{H}_2\text{O})_4]$ (**2**) was reduced by certain metallocenes. By comparing isostructural salts of $[\text{Mn}_{12}]^-$ anions with and without a magnetic cation, it is possible to determine the effect of magnetic cation on the magnetization behavior of $[\text{Mn}_{12}]^-$ complexes. Here we report the magnetic properties of the $[\text{Mn}_{12}]^-$ complexes with paramagnetic $[\text{Fe}(\text{C}_5\text{Me}_5)_2]^+$ cations and with non-magnetic $[\text{Co}(\text{C}_5\text{Me}_5)_2]^+$ cations.

2. Experimental

2.1. Compound preparation

All chemicals and solvents were used as received; all preparations and manipulations were performed under argon atmosphere using Schlenk techniques. Bis(pentamethylcyclopentadienyl)iron was purchased from Aldrich Chemical Co. Bis(pentamethylcyclopentadienyl)cobaltocenium hexafluorophosphate was purchased from Strem Chemicals and converted to $\text{Co}(\text{C}_5\text{Me}_5)_2$ by a literature procedure [10]. The Mn_{12} -acetate (**1**) was prepared by the literature method [11]. Neutral complex $[\text{Mn}_{12}\text{O}_{12}(\text{O}_2\text{CC}_6\text{H}_4\text{F}(-o))_{16}(\text{H}_2\text{O})_4]$ (**2**) was prepared using the ligand substitution method described elsewhere [12].

2.2. $[\text{PPh}_4][\text{Mn}_{12}\text{O}_{12}(\text{O}_2\text{CC}_6\text{H}_4\text{F}(-o))_{16}(\text{H}_2\text{O})_4]$ (**2a**)

A method similar to that described in the literature [12] was used. To a stirred dark brown solution of complex **2** (100 mg, 0.027 mmol) in CH_2Cl_2 (10 ml) was added solid PPh_4I (12 mg, 0.026 mmol). The solution was stirred for an additional 10 min with no noticeable color change. Hexanes (20 ml) were then added, and the flask was left undisturbed for several days at ambient temperature. The brown powder at the bottom was collected by decantation and washed with hexanes. The yield was 43%.

2.3. $[\text{Fe}(\text{C}_5\text{Me}_5)_2][\text{Mn}_{12}\text{O}_{12}(\text{O}_2\text{CC}_6\text{H}_4(o-F))_{16}(\text{H}_2\text{O})_4]$ (**2b**)

Complex **2** (100 mg, 0.027 mmol) was dissolved in CH_2Cl_2 (5 ml). An equivalent amount of bis(pentamethylcyclopentadienyl)iron (8.6 mg, 0.026 mmol) dissolved in CH_2Cl_2 (3 ml) was added to the above solution and stirred for 10 min. To the resultant solution 10 ml of hexanes was added slowly. Several days later, brown-black needle crystals were obtained. The yield was 60%. *Anal.* Found: C, 44.87; H, 3.07; N, 0.00. Calc. for $\text{C}_{133}\text{H}_{104}\text{Cl}_2\text{F}_{16}\text{FeMn}_{12}\text{O}_{48}$ (as **2b**· CH_2Cl_2): C, 44.87; H, 2.94; N, 0.00%.

2.4. $[\text{Co}(\text{C}_5\text{Me}_5)_2][\text{Mn}_{12}\text{O}_{12}(\text{O}_2\text{CC}_6\text{H}_4(o-F))_{16}(\text{H}_2\text{O})_4]$ (**2c**)

The method described above was used. After standing for several days, brown-black needle crystals were obtained. The yield was 65%. *Anal.* Found: C, 43.80; H, 2.68; N, 0.00. Calc. for $\text{C}_{134}\text{H}_{106}\text{Cl}_4\text{CoF}_{16}\text{Mn}_{12}\text{O}_{48}$ (as **2c**· $2\text{CH}_2\text{Cl}_2$): C, 44.12; H, 2.93; N, 0.00%.

2.5. Physical measurements

DC magnetic susceptibility data were collected on microcrystalline or a single-crystal sample restrained in eicosane to prevent torquing on a Quantum Design MPMS5 SQUID magnetometer equipped with a 5.5 T magnet. A diamagnetic correction to the observed susceptibilities was applied using Pascal's constants. Alternating current (ac) susceptibility measurements were carried out on a Quantum Design MPMS2 SQUID magnetometer equipped with a 1 T magnet and capable of achieving temperatures of 1.7–400 K. The magnitude of ac field is fixed at 0.1 mT, oscillating at a frequency in the range of 5–1000 Hz. Magnetization hysteresis loops were collected on a Quantum Design MPMS5 SQUID magnetometer employing oriented single crystals. Sample alignments in eicosane were performed while keeping the samples in a 5.0 T field at a temperature above the melting point (308–312 K) of eicosane for 15 min, after which the temperature was gradually decreased below the melting point to solidify the eicosane in order to constrain the sample. In this way we could measure hysteresis loops with the external magnetic field applied parallel to the easy axis of magnetization. In case of a measurement with a magnetic field applied perpendicularly to the easy axis of magnetization, a sample prepared as described above was rotated 90° in the sample holder. Applied magnetic fields were varied from 2.5 to –2.5 T to generate hysteresis loops.

3. Results and discussion

3.1. Reduced $[\text{Mn}_{12}]^-$ complexes characterized by ac magnetic susceptibility

Ferrocene is known to have sufficient redox potential to reduce some $[\text{Mn}_{12}]^-$ complexes [12]. Decamethylferrocene and decamethylcobaltocene were employed in an one-electron reduction of $[\text{Mn}_{12}\text{O}_{12}(\text{O}_2\text{CC}_6\text{H}_4\text{F}(-o))_{16}(\text{H}_2\text{O})_4]$. The reduction products were subjected to ac susceptibility measurements to investigate their magnetic responses. It is well known that a SMM shows a frequency-dependent out-of-phase ac susceptibility signal (χ''_M). Figs. 1–3 show plots of $\chi'_M T$ vs T (top) and χ''_M vs T (bottom) for complexes

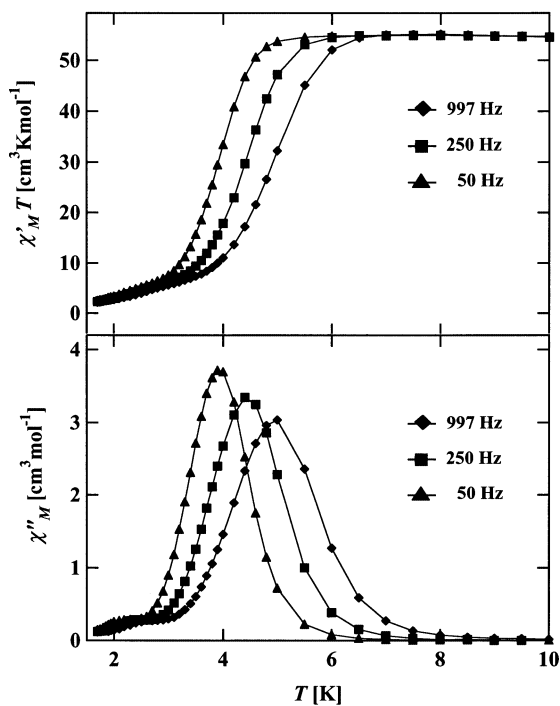


Fig. 1. Plots of $\chi'_M T$ vs T (top) and χ''_M vs T (bottom) for a microcrystalline sample of complex **2a** in a 0.1 mT ac field oscillating at the indicated frequencies, where χ'_M and χ''_M are the in-phase and the out-of-phase magnetic susceptibilities, respectively.

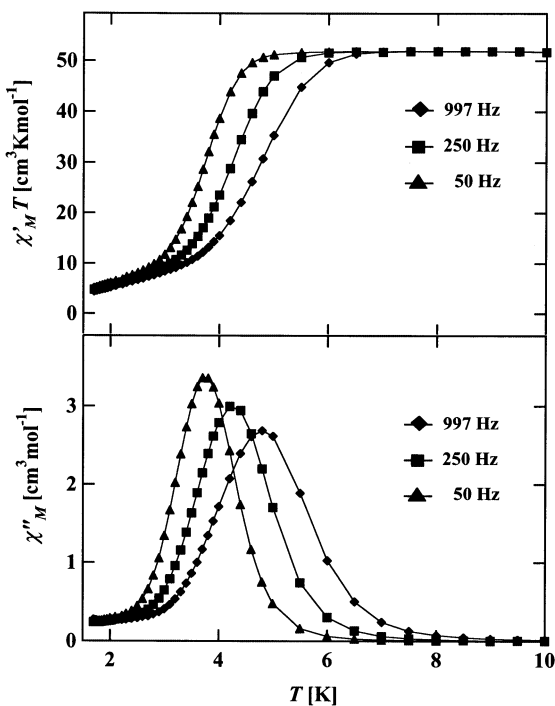


Fig. 2. Plots of $\chi'_M T$ vs T (top) and χ''_M vs T (bottom) for a polycrystalline sample of complex **2b** in a 0.1 mT ac field oscillating at the indicated frequencies, where χ'_M and χ''_M are the in-phase and the out-of-phase magnetic susceptibilities, respectively.

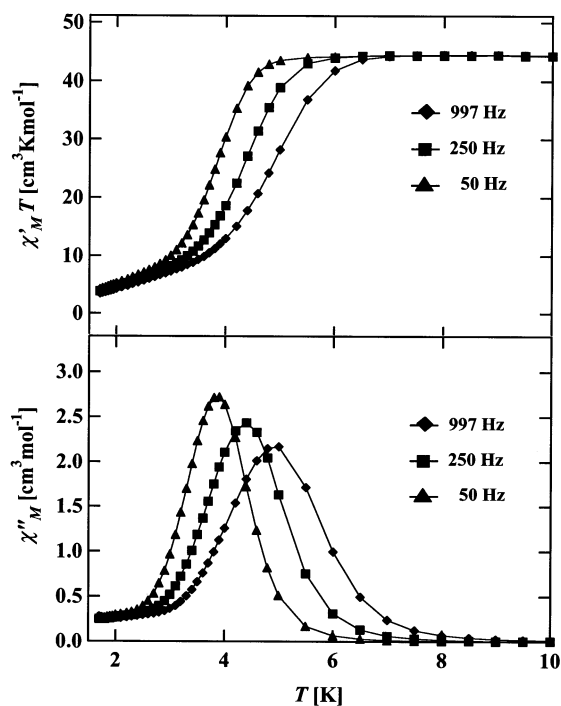


Fig. 3. Plots of $\chi'_M T$ vs T (top) and χ''_M vs T (bottom) for a polycrystalline sample of complex **2c** in a 0.1 mT ac field oscillating at the indicated frequencies, where χ'_M and χ''_M are the in-phase and the out-of-phase magnetic susceptibilities, respectively.

[PPh₄][Mn₁₂O₁₂(O₂CC₆H₄F(-o))₁₆(H₂O)₄], [Fe(C₅Me₅)₂]-[Mn₁₂O₁₂(O₂CC₆H₄(o-F))₁₆(H₂O)₄], and [Co(C₅Me₅)₂]-[Mn₁₂O₁₂(O₂CC₆H₄(o-F))₁₆(H₂O)₄], respectively, where χ'_M is the in-phase ac susceptibility. Since one peak is observed in the 3–6 K range in the frequency range of 50–997 Hz, we can conclude there is only one magnetization relaxation process seen for each of these salts.

The presence of frequency-dependent out-of-phase ac signals indicate complexes **2a–2c** function as SMMs. Fig. 4 shows a double-well potential energy diagram for an $S = 21/2$ SMM reversing its magnetization from spin “up” to spin “down”. The ground state of an SMM is split by axial zero-field splitting; the spin Hamiltonian can be expressed in its simplest form as given in Eq. (1):

$$\hat{H} = g\mu_B(\hat{H} \cdot \hat{S}) + D[\hat{S}_z^2 - \frac{1}{3}S(S+1)] \quad (1)$$

where μ_B is the Bohr magneton and g is Lande’s factor. The first term is the Zeeman term and the second is the axial zero-field interaction term. The parameter D gauges the axial zero-field splitting of the ground state. Since the energy of each M_s sublevel of the ground state is given as $E = M_s g\mu_B H + D[M_s^2 - \frac{1}{3}S(S+1)]$, the potential energy barrier U at the external field $H = 0$ is given by $U = |D|(S_z^2 - 1/4)$. At the χ''_M peak temperature, the rate of spin flip of the magnetic moment of a molecule between the “up” and “down” states is synchronized to the ac frequency.

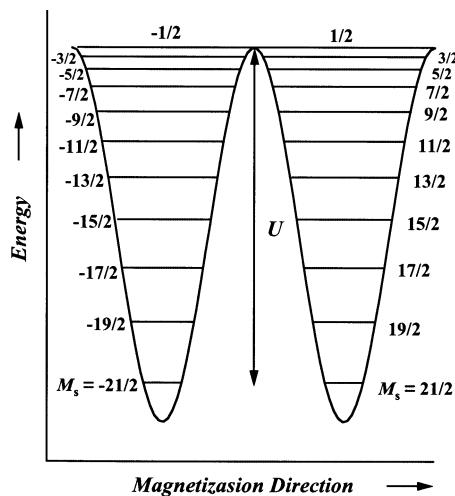


Fig. 4. Plot of the potential energy vs the magnetization direction for a single-molecule magnet with an $S = 21/2$ ground state split by axial zero-field splitting. The potential energy barrier U is equal to $|D|(S_z^2 - 1/4)$.

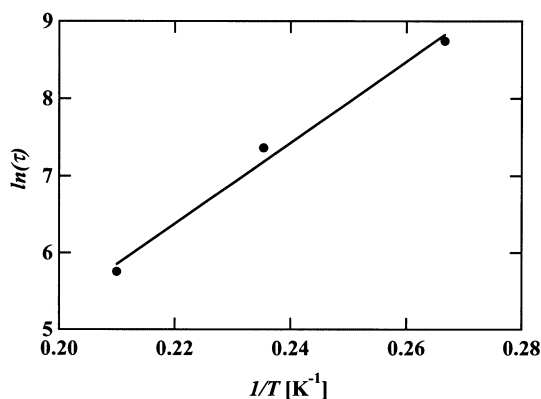


Fig. 5. Plot of the natural logarithm of the magnetization relaxation rate $\ln(\tau)$ vs the inverse of the absolute temperature for complex **2b**. The solid line represents a least-squares fit of the data to the Arrhenius equation (see text).

The frequency dependence of the χ''_M peak temperature can be analyzed by the Arrhenius law. On the basis of the plots of the natural logarithm of the relaxation time τ evaluated from $1/(2\pi\nu)$, where ν is the ac fre-

quency, versus the inverse of the χ''_M peak temperature T , the effective energy barrier U_{eff} and pre-exponential factor τ_0 can be estimated by the following equation [13]:

$$\tau = \tau_0 \exp\left(\frac{U_{\text{eff}}}{k_B T}\right) \quad (2)$$

where k_B is the Boltzmann constant. The Arrhenius plot for complex **2b** is shown in Fig. 5, where the solid line shows the result of a least-squares fit of the ac susceptibility relaxation data to Eq. (2). For complex **2b**, the effective energy barrier is $U_{\text{eff}} = 51.6$ K with pre-exponential factor of 3.4×10^{-9} s. Table 1 lists the results of the ac susceptibility and relaxation fitting data for the three complexes studied. At 1 kHz ac frequency, the anionic complexes **2a**, **2b**, and **2c** show χ''_M peaks at 5.0, 4.8, and 5.1 K, respectively, while the parent neutral complex **2** shows a χ''_M peak at 6.1 K. The effective energy barriers U_{eff} were evaluated to be 57, 52, and 52 K for complexes **2a**, **2b**, and **2c**, respectively. These values are somewhat smaller than those obtained for neutral complexes **1** and **2**, but are comparable to those of anionic $[\text{Mn}_{12}]^-$ SMMs such as $[\text{PPh}_4][\text{Mn}_{12}\text{O}_{12}(\text{O}_2\text{CET})_{16}(\text{H}_2\text{O})_4]$ (60.2 K [14]) and $[\text{PPh}_4][\text{Mn}_{12}\text{O}_{12}(\text{O}_2\text{CPh})_{16}(\text{H}_2\text{O})_4]$ (55 [9], 57.5 K [15]).

It is noteworthy that in the ac susceptibility responses of complexes **2a–2c**, there is no or very small contribution of an LT phase that is usually observed together with the HT phase signal [12]. The three complexes show predominantly a HT phase signal independent of the magnetism of the counter cations. This is in contrast to the result reported for $[m\text{-MPYNN}][\text{Mn}_{12}\text{O}_{12}(\text{O}_2\text{CPh})_{16}(\text{H}_2\text{O})_4]$ [9], where the magnetic cation seems to have a drastic influence on the magnetization relaxation of the $[\text{Mn}_{12}]^-$ anion.

3.2. Magnetization hysteresis loops

Recently, magnetization hysteresis loops (M vs H) have been observed for SMMs including several $[\text{Mn}_{12}]^-$ complexes [6,14,16–21], $[\text{Fe}_8\text{O}_2(\text{OH})_{12}(\text{tacn})_6]^{8+}$ [22], (tacn = triazacyclononane) and

Table 1
Magnetization relaxation parameters for several $[\text{Mn}_{12}]$ SMMs

Complexes	Charge of $[\text{Mn}_{12}]$	Peak temperature (K) in χ''_M at 1 kHz	U_{eff}/k_B (K) ^a	τ_0 (s) ^a	Notes
1	0	7.3 ^b	61	2.1×10^{-7}	Refs. [3,6]
2	0	6.1	65	3.8×10^{-9}	this work
2a	-1	5.0	57	1.6×10^{-9}	this work
2b	-1	4.8	52	3.4×10^{-9}	this work
2c	-1	5.1	52	5.6×10^{-9}	this work
Mn_{12} -benzoate- <i>m</i> -MPYNN ^c	-1	3.9 ^b	50	3.0×10^{-10}	Ref. [9]

^a Estimated from Arrhenius plots using Eq. (2).

^b Extrapolated to 1 kHz ac frequency using original data.

^c *m*-MPYNN: *m*-*N*-methylpyridinium nitronitroxide.

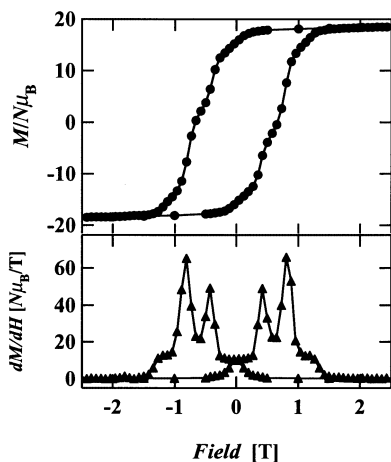


Fig. 6. Top: magnetization hysteresis loop measured at 1.85 K for powder sample of **2a**. Samples were oriented in eicosane wax matrixes. Bottom: the first derivative of the magnetization hysteresis loop.

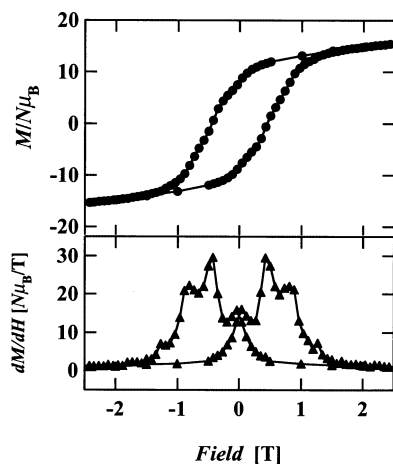


Fig. 7. Top: magnetization hysteresis loop measured at 1.85 K for microcrystalline sample of **2b**. Samples were oriented in eicosane wax matrixes. Bottom: the first derivative of the magnetization hysteresis loop.

$[\text{Mn}_4\text{O}_3\text{Cl}(\text{O}_2\text{CCH}_3)_3(\text{dbm})_3]$ [23] (dbm = dibenzoyl-methane monoanion). Steps are observed at relatively constant intervals of field. These steps in magnetization are due to a sudden increase in the decay rate of magnetization occurring at specific field values and have been attributed to field-tuned quantum tunneling of the magnetization. The observation of quantum tunneling of magnetization in complexes with not only integer spin but also with half-integer spin ground states indicates a transverse internal field plays an important role in the tunneling process [21,23].

The magnetization hysteresis loop measured for complex **2a** at 1.85 K is shown in Fig. 6. The magnetization saturates completely at fields above 1.4 T to approximately $18 N\mu_B$. Hysteresis is seen with a coercive field of 0.66 T. In the lower part of Fig. 6 is shown the first

derivative of the hysteresis plot. As the field is decreased from +2 T, the first step can be seen at zero field, followed by steps at -0.42 and -0.81 T. On the other hand, the magnetization hysteresis behaviors of complexes **2b** and **2c** are somewhat different from that of complex **2a**. The magnetization hysteresis loops of complexes **2b** and **2c** obtained at 1.85 K are shown in Figs. 7 and 8, respectively. Although they show hysteresis with coercive fields of 0.45 and 0.41 T, respectively, the magnetization curves are not completely saturated up to 2.5 T. These facts imply the magnetization easy axes of $[\text{Mn}_{12}]^-$ anions in each compound are not fully parallel to the external field, probably due to the presence of two or more orientations of $[\text{Mn}_{12}]^-$ anions in the crystallographic unit cell. In the lower parts of Figs. 7 and 8, which show the first derivative of the hysteresis plots, steps in the hysteresis loop can be seen at -0.04 , -0.42 , and -0.81 T for both complexes **2b** and **2c**. The step interval ΔH is estimated to be 0.39 T for both complexes, which is the same as that of complex **2a**. The steps correspond to increases in the rate of change of the magnetization, and are attributable to resonant tunneling between quantum spin states. With the spin Hamiltonian of Eq. (1), the step interval ΔH in a hysteresis loop is given as $\Delta H = -nD/(g\mu_B)$, where $n = 0, 1, 2, \dots$. Using the observed step interval ΔH of 0.39 T for three complexes, we can estimate that the ratio $|D|/g$ is equal to 0.27.

There is no effect of paramagnetism from the Fe(III) ion ($S = 1/2$) in the $[\text{Fe}(\text{C}_5\text{Me}_5)_2]^+$ cation on the magnetization behavior of the $[\text{Mn}_{12}]^-$ anion as far as the magnetization hysteresis measurement is concerned. The observed differences of magnetization saturation behavior between complexes **2a** and **2b** or **2c** are probably due to the crystal packing effects induced by differences in the sizes and shapes of the cations.

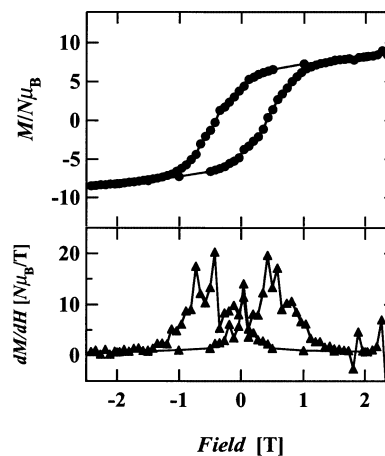


Fig. 8. Top: magnetization hysteresis loop measured at 1.85 K for microcrystalline sample of **2c**. Samples were oriented in eicosane wax matrixes. Bottom: the first derivative of the magnetization hysteresis loop.

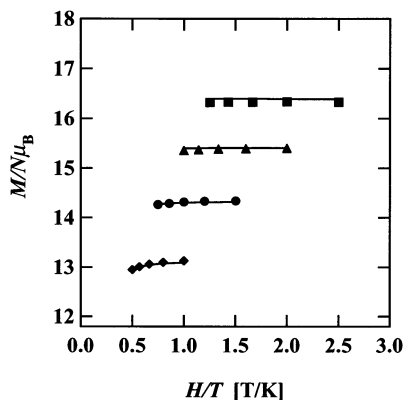


Fig. 9. Plot of the reduced magnetization $M/(N\mu_B)$ vs the ratio of the external field and the absolute temperature for **2a**. The solid lines are fits of the data to an $S = 21/2$ state with $g = 1.95$ and $D = -0.55$ K. The data were measured at 2 (◆), 3 (●), 4 (▲), and 5 T (■).

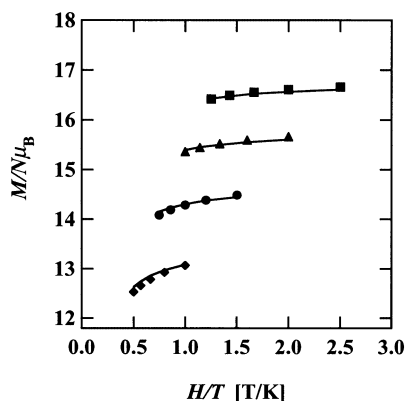


Fig. 10. Plot of the reduced magnetization $M/(N\mu_B)$ vs the ratio of the external field and the absolute temperature for **2b**. The solid lines are fits of the data to an $S = 19/2$ state with $g = 1.96$ and $D = -0.54$ K in the presence of $[\text{Fe}(\text{C}_5\text{Me}_5)_2]^+$ cation ($S = 1/2$, $g_{\parallel} = 4.43$, $g_{\perp} = 1.35$). The data were measured at 2 (◆), 3 (●), 4 (▲), and 5 T (■).

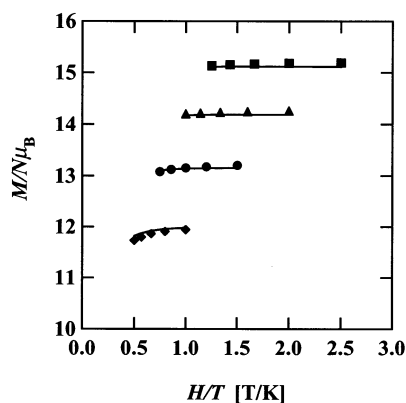


Fig. 11. Plot of the reduced magnetization $M/(N\mu_B)$ vs the ratio of the external field and the absolute temperature for **2c**. The solid lines are fits of the data to an $S = 19/2$ state with $g = 1.96$ and $D = -0.57$ K. The data were measured at 2 (◆), 3 (●), 4 (▲), and 5 T (■).

3.3. DC magnetization versus magnetic field

In order to estimate the ground spin state and the magnitude of the zero-field splitting for the $[\text{Mn}_{12}]^-$ complexes, dc magnetization data were collected in the temperature range of 2.0–4.0 K and at external fields of 2.0, 3.0, 4.0, and 5.0 T for polycrystalline samples. To avoid torquing during measurements, samples were fixed with eicosane wax without applying magnetic field before measurements. The observed magnetization data $M/(N\mu_B)$ for complexes **2a**, **2b**, and **2c** are plotted vs H/T in Figs. 9–11, respectively. A spin Hamiltonian including an isotropic Zeeman interaction and axial zero-field splitting (DS_z^2) was used to least-squares-fit the data by assuming that only the ground state is populated in the 2.0–4.0 K and 2.0–5.0 T ranges. The contribution of the paramagnetic $[\text{Fe}(\text{C}_5\text{Me}_5)_2]^+$ cations ($S = 1/2$, $g_{\parallel} = 4.43$, $g_{\perp} = 1.35$) is also included for complex **2b**. The matrix was diagonalized on each cycle, and a powder average was calculated. TIP was held fixed at $2400 \times 10^{-6} \text{ cm}^3 \text{ mol}^{-1}$.

The reduced magnetization data for complex **2a** were fitted assuming an $S = 21/2$ ground state. The lines in Fig. 9 show the fitting with the parameters of $g = 1.96$ and $D = -0.56$ K. If we assume an $S = 19/2$ ground state, the best-fit parameters were $g = 1.89$ and $D = -0.35$ K. Although the $[\text{Mn}_{12}]^-$ anions reported before [12,14,15] have been shown to have an $S = 19/2$ ground state, it is not so surprising for the $[\text{Mn}_{12}]^-$ anion to have an $S = 21/2$ ground state. Because one-electron reduction changes an Mn (III) ion with $S = 2$ to an Mn (II) ion with $S = 5/2$, which leads to a simple vector-sum calculation of $(7 \times 2 + 5/2) - 4 \times 3/2 = 21/2$, if the Mn ion maintains similar magnetic interaction with the neighboring Mn ions. The validity of the $S = 21/2$ ground state for complex **2a** is also exemplified by the comparison between U and U_{eff} . By using D and S , we can estimate the energy barrier $U = |D|(S_z^2 - 1/4)$. The estimated U of 31.2 K for the $S = 19/2$ ground state is appreciably smaller than the effective energy barrier U_{eff} of 57 K obtained by ac susceptibility measurements. On the other hand, the U of 62 K for the $S = 21/2$ ground state is larger than U_{eff} , which is consistent with the thermally assisted tunneling model [24]. In this model, the system initially in the left well in Fig. 4 is thermally activated to a fast-tunneling level near the top of the barrier, tunnels across and then spontaneously decays into the ground state in the right well. This explains why $U_{\text{eff}} < U$. High-frequency EPR data are being collected to confirm that complex **2a** has a $S = 21/2$ ground state.

The reduced magnetization data for complex **2b** were fitted assuming either an $S = 19/2$ or an $21/2$ ground state. The best fit for the $S = 19/2$ ground state occurred for parameters of $g = 1.91$ and $D = -0.48$ K. If we assume an $S = 21/2$ ground state, the best fit was obtained with parameters of $g = 1.73$ and $D = -0.39$

K. Although the fittings are quite good for either the $S = 19/2$ or the $S = 21/2$ ground state possibilities, it is reasonable to conclude the $S = 19/2$ ground state for complex **2b** because the g -value of 1.73 for the $S = 21/2$ ground state is too small compared to the reported g -values for $[\text{Mn}_{12}]^-$ complexes [4,15,25].

However, the estimated U for the $S = 19/2$ ground state was 44 K which is a little smaller than U_{eff} of 52 K obtained by the ac magnetization relaxation experiments. In order to find more reasonable parameters, the contour plot of the error χ^2 as a function of g and D for the $S = 19/2$ ground state is shown in Fig. 12. There is a narrow area with χ^2 lower than 0.05. The boundary of this area spreads from $(g, D/\text{K}) = (1.96, -0.54)$ to $(g, D/\text{K}) = (1.86, -0.41)$. If we choose the former point as a better fit, we can obtain more reasonable U (49 K). The lines in Fig. 10 show the fitting with the parameters of $g = 1.96$ and $D = -0.54$ K for the $S = 19/2$ ground state.

Similar analysis was performed on the reduced magnetization data of complex **2c**. The situation was almost the same as the case for complex **2b**. The lines in Fig. 11 show the fitting with parameters of $g = 1.95$ and $D = -0.57$ K for an $S = 19/2$ ground state. The possibility of an $S = 21/2$ ground state is not reasonable because the g -value of 1.72 is too small. A contour plot for the $S = 19/2$ ground state is similar to Fig. 12. The above parameters are consistent with respect to U (51 K), although the best fit to the reduced magnetization data was obtained with the parameters $g = 1.90$ and $D = -0.50$ K.

These analyses show that g and D parameters are similar to each other for these three complexes (**2a**: $g = 1.96$, $D = -0.56$ K; **2b**: $g = 1.96$, $D = -0.54$ K; **2c**: $g = 1.95$, $D = -0.57$ K) in spite of the difference in spin ground states ($S = 21/2$ for **2a** and $S = 19/2$ for **2b** and **2c**). This is consistent with the observation of the

same step interval ΔH in the hysteresis loops for all three complexes. The ratio $|D|/g$ of 0.27 estimated from ΔH is very close to those calculated by using the above parameters: 0.29, 0.28, and 0.29 for complexes **2a**, **2b**, and **2c**, respectively, indicating the validity of the above analyses. The assignments of the spin ground states for these complexes are also supported by U_{eff} values estimated from the ac susceptibility measurements. The largest U_{eff} of 57 K for complex **2a** in the three is ascribed to the largest spin ground state $S = 21/2$ for the three. The paramagnetism of the $[\text{Fe}(\text{C}_5\text{Me}_5)_2]^+$ cation has essentially no effect on the ground state spin S nor parameters g and D of the $[\text{Mn}_{12}]^-$ anion.

4. Concluding remarks

The results presented show that the effect of the paramagnetic metallocene cation on the magnetic properties of the $[\text{Mn}_{12}]^-$ SMM is negligibly small, which is in contrast to a result reported by Takeda and Awaga [9]. They concluded that the organic radical cation enhances the magnetization relaxation of the $[\text{Mn}_{12}]^-$ -benzoate anion. However, on the basis of the results presented here, the magnetic cation does not influence the magnetic property of $[\text{Mn}_{12}]^-$ anion.

Acknowledgements

This work was supported by NSF grants to D.N.H. and G.C. The ac susceptibility measurements were performed with an AC SQUID susceptometer provided by the Center for Interface and Material Science, funded by the W.A. Keck Foundation.

References

- [1] E.M. Chudnovsky, *Science* 274 (1996) 938.
- [2] B. Schwarzschild, *Phys. Today* January (1997) 17.
- [3] R. Sessoli, D. Gatteschi, A. Caneschi, M.A. Novak, *Nature* 365 (1993) 141.
- [4] R. Sessoli, H.-L. Tsai, A.R. Schake, S. Wang, J.B. Vincent, K. Folting, D. Gatteschi, G. Christou, D.N. Hendrickson, *J. Am. Chem. Soc.* 115 (1993) 1804.
- [5] D. Gatteschi, A. Caneschi, L. Pardi, R. Sessoli, *Science* 265 (1994) 1054.
- [6] J.R. Friedman, M.P. Sarachik, J. Tejada, R. Ziolo, *Phys. Rev. Lett.* 76 (1996) 3830.
- [7] J.R. Friedman, M.P. Sarachik, J.M. Hernandez, X.X. Zhang, J. Tejada, E. Molins, R. Ziolo, *J. Appl. Phys.* 81 (1997) 3978.
- [8] J.M. Hernandez, X.X. Zhang, F. Luis, J. Tejada, J.R. Friedman, M.P. Sarachik, R. Ziolo, *Phys. Rev. B* 55 (1997) 5858.
- [9] K. Takeda, K. Awaga, *Phys. Rev. B* 56 (1997) 14 560.
- [10] J.L. Robbins, M. Edelstein, B. Spencer, J.C. Smart, *J. Am. Chem. Soc.* 104 (1982) 1882.
- [11] T. Lis, *Acta Crystallogr., Sect. B* 36 (1980) 2042.

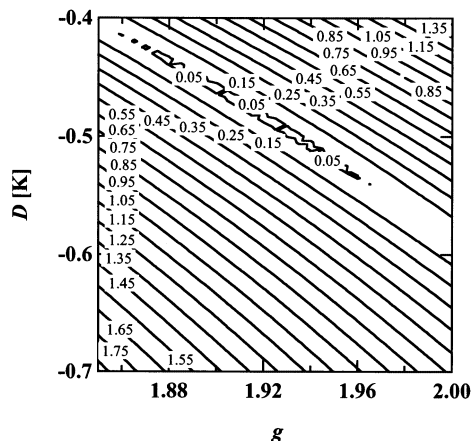


Fig. 12. Contour plot of least-squares fitting parameter (χ^2) as a function of g and D in fitting the reduced magnetization data for complex **2b** with the $S = 19/2$ ground state.

- [12] H.J. Eppley, H.-L. Tsai, N.D. Vries, K. Folting, G. Christou, D.N. Hendrickson, *J. Am. Chem. Soc.* 117 (1995) 301.
- [13] S.M.J. Aubin, M.W. Wemple, D.A. Adams, H.-L. Tsai, G. Christou, D.N. Hendrickson, *J. Am. Chem. Soc.* 118 (1996) 7746.
- [14] S.M.J. Aubin, S. Spagna, H.J. Eppley, R.E. Sager, G. Christou, D.N. Hendrickson, *Chem. Commun.* (1998) 803.
- [15] S.M.J.Z.S. Aubin, L.A. Pardi, J. Krzystek, K. Folting, L.-C. Brunel, A.L. Rheingold, G. Christou, D.N. Hendrickson, *Inorg. Chem.* 38 (1999) 5329.
- [16] J.R. Friedman, M.P. Sarachik, J. Tejada, J. Maciejewski, R. Ziolo, *J. Appl. Phys.* 79 (1996) 6031.
- [17] L. Thomas, F. Lioni, R. Ballou, D. Gatteschi, R. Sessoli, B. Barbara, *Nature* 383 (1996) 145.
- [18] S.M.J. Aubin, Z. Sun, I.A. Guzei, A.L. Rheingold, G. Christou, D.N. Hendrickson, *Chem. Commun.* (1997) 2239.
- [19] S.M.J. Aubin, S. Spagna, H.J. Eppley, R.E. Sagel, K. Folting, G. Christou, D.N. Hendrickson, *Mol. Cryst. Liq. Cryst.* 305 (1997) 181.
- [20] D. Ruiz, Z. Sun, B. Albel, K. Folting, J. Ribas, G. Christou, D.N. Hendrickson, *Angew. Chem., Int. Ed. Engl.* 37 (1998) 300.
- [21] S.M.J. Aubin, N.R. Dilley, M.W. Wemple, M.B. Maple, G. Christou, D.N. Hendrickson, *J. Am. Chem. Soc.* 120 (1998) 839.
- [22] C. Sangregorio, T. Ohm, C. Paulsen, R. Sessoli, D. Gatteschi, *Phys. Rev. Lett.* 78 (1997) 4645.
- [23] S.M.J. Aubin, N.R. Dilley, L. Pardi, J. Krzystek, M.W. Wemple, L.-C. Brunel, M.B. Maple, G. Christou, D.N. Hendrickson, *J. Am. Chem. Soc.* 120 (1998) 4991.
- [24] M.A. Novak, R. Sessoli, in: L. Gunther, B. Barbara (Eds.), *Quantum Tunneling of Magnetization — QTM'94*, Kluwer, Dordrecht, 1995, pp. 171–188.
- [25] A. Caneschi, D. Gatteschi, R. Sessoli, A.L. Barra, L.-C. Brunel, M. Guillot, *J. Am. Chem. Soc.* 113 (1991) 5873.